CHAPTER 5

The Principle of Maximum Entropy in Image Recovery

*Xinhua Zhuang**

Coordinated Science Laboratory
University of Illinois at
Champaign-Urbana
Urbana, Illinois 61801

Einar Østevold

Norwegian Defense Research
Establishment
N-2007 Kjeller, Norway

Robert M. Haralick

Machine Vision International
Ann Arbor, Michigan 48104

5.1 INTRODUCTION

For many decades it has been recognized, or conjectured, that the notion of entropy defines a kind of measure on the space of probability distributions, such that those of high entropy are in some sense favored over others, all other things being equal. The basis for this was stated first in a variety of intuitive forms: that distributions of higher entropy represent more "disorder," that they are "smoother," "more probable," "less predictable," that they "assume less" and hence "are more natural" according to Shannon's interpretation of entropy as an information measure, etc.

While each of these points of view doubtless reflects an element of truth, none seems explicit enough to lend itself to a quantitative demonstration of the kind we are accustomed to having in other fields of applied mathematics. Accordingly, many approaching this field are disconcerted by what they sense as a kind of vagueness, the underlying theory lacking a solid content.

* Visiting Professor, People's Republic of China.

This has not prevented the fruitful exploitation of this property of entropy. The maximum entropy (ME) principle, briefly speaking, is: when we make inferences based on incomplete information, we should draw them from that probability distribution that has the maximum entropy allowed by the information we do have. Jaynes [1,2] has been a foremost proponent of maximum entropy prior distributions consistent with known information.

Essentially all of the known results of statistical mechanics, equilibrium and nonequilibrium, are derivable consequences of this principle. In image restoration and spectrum analysis, the maximum entropy principle takes into account cogent information about multiplicities that orthodox statistics misses because of its failure to admit prior probabilities.

Perhaps Frieden [3] was the first one to correctly pose one type of maximum entropy image restoration problem. In his statistical model, the image space is divided into n resolution cells (or n events). The frequency of occurrence of the ith event is identified with

$$p_i = f_i \Big/ \sum_{i=1}^{n} f_j,$$

where f_i represents the gray tone intensity in the ith cell. Thus, the entropy is defined as

$$H(p_1, \ldots, p_n) = -\sum_{i=1}^{n} p_i \log p_i.$$

Apart from Frieden's statistical model, the maximization of $H(f_1, \ldots, f_n)$,

$$H(f_1, \ldots, f_n) = -\sum_{i=1}^{n} f_i \log f_i, \tag{5.1-1}$$

does have a smoothing influence on the restored image f_i, $i = 1, \ldots, n$, assuming the sum of gray levels $\sum_{i=1}^{n} f_i = t$ is a known constant. To show the smoothing influence we show that as f_i and f_j approach each other while t stays the same, $H(f_1, \ldots, f_n)$ will increase. Assume that $f_i > f_j$; thus for the two pixels to approach each other in value while t continues to be the same, we may introduce the following changes:

$$\nabla f_i = -\varepsilon, \qquad \nabla f_j = \varepsilon, \tag{5.1-2}$$

as $\varepsilon \to 0$. After these changes, we can calculate the new summation in Eq. (5.1-1) denoted by H':

$$\begin{aligned} H' &= H(f_1, \ldots, f_n) + f_i \log f_i + f_j \log f_j \\ &\quad -(f_i - \varepsilon) \log(f_i - \varepsilon) - (f_j + \varepsilon) \log(f_j + \varepsilon) \\ &= (f_1, \ldots, f_n) + \varepsilon \log(f_i / f_j) \\ &> H(f_1, \ldots, f_n), \end{aligned} \tag{5.1-3}$$

where we have used the approximate formula

$$\log(1 + x) = x, \qquad |x| \ll 1.$$

Besides maximizing $H(f_1, \ldots, f_n)$, many other image restoration procedures exert a smoothing influence on the solution. In fact, various linear techniques can be used to improve the resolution of a blurred image of an object. However, the linear techniques often induce erroneous detail such as oscillations or "ringing" around sharp changes in intensity in the image. That is a particular problem with images of complex objects since the superposition of many oscillations can give spurious detail with unpredictable shapes and intensities. Therefore, a "safe" inversion technique is required—one giving restorations free from ringing, such that confidence can be placed in the reality of all extra details revealed by the restoration method. Naturally, interest has centered on nonlinear techniques which incorporate constraints to reduce the artifacts generated in the restoration. Of the nonlinear techniques, maximum entropy is a fundamental method for the solution of the inversion problems in image restoration. A variety of iterative algorithms have been proposed to obtain the maximum entropy solution.

The computing times required by most of the these algorithms are, however, much higher than those required by linear methods, and this has often procluded their use on images containing more than 64×64 pixels. Therefore, designing more efficient algorithms becomes crucial.

Section 5.2 introduces Frieden's statistical model for an "object" in optical image formation and a maximum entropy image restoration algorithm which requires solving $m + 1$ nonlinear equations with $m + 1$ unknowns, where m represents the number of observed data values.

Section 5.3 introduces Burch *et al*/[4] algorithm, which requires solving a optimization problem in $(n + 1)$-dimensional space.

In Section 5.4 we present our own technique [5]. This is a differential equation approach to the ME restoration problem. The problem is reduced to solving a system of differential equations with easily obtained initial conditions. Instead of doing an $(n + 1)$-dimensional search as required by most ME techniques, a one-dimensional search along a well-defined path in the $(n + 1)$-dimensional space is performed. The search path is defined by the Cauchy problem of differential equations. Results are shown for cases with strong deblurring and for cases with high noise levels. Our results are compared with those produced by competing ME techniques. The aspect of computational cost is also discussed.

Section 5.5 is the conclusion.

5.2 FRIEDEN'S APPROACH [3]

Frieden's approach is based on a statistical model for an "object" in optical image formation. The object is defined as an unknown spatial radiance distribution $f_i = f(x_i)$, $i = 1, \ldots, n$, which produces an image irradiance distribution $d_j = d(y_j)$, $j = 1, \ldots, m$, which is collected as data. The connection between f and d is given by

$$d_j = \sum_{i=1}^{n} A_{ji} f_i + e_j, \qquad j = 1, \ldots, m, \tag{5.2-1}$$

where $e_j = e(y_j)$ denotes noise. Here, the object is imagined to be composed of discrete, mathematical "grains" of small intensity Δ which are distributed over the object scene. The scene is subdivided into cells centered on a subdivision of points $\{x_i\}$, $i = 1, \ldots, n$, and the unknown object is assumed to have g_i grains in cell i. Thus $f(x_i) = \Delta \cdot g_i$. Let p_i represent the probability of a grain locating in cell i. Then if a large number of grains are distributed over the object, by the law of large numbers

$$p_i = g_i / g_T,$$

where g_T is the total number of grains in the object; g_T is assumed known by conservation of energy from the image data.

The entropy, from information theory, is defined as

$$\begin{aligned} H(p_1, \ldots, p_n) &\triangleq -\sum_{i=1}^{n} p_i \log p_i \\ &= -\sum_{i=1}^{n} \left(\frac{g_i}{g_T}\right) \log\left(\frac{g_i}{g_T}\right) \\ &= -\sum_{i=1}^{n} \left(\frac{f_i}{\sum_{i=1}^{n} f_i}\right) \log\left(\frac{f_i}{\sum_{i=1}^{n} f_i}\right) \\ &= -\frac{\sum_{i=1}^{n} f_i \log f_i}{\sum_{i=1}^{n} f_i} - \log\left(\sum_{i=1}^{n} f_i\right). \end{aligned} \tag{5.2-2}$$

Since the total spatial radiances $\sum_{i=1}^{n} f_i \; (= \Delta \cdot g_T)$ is a constant, the principle of maximum entropy then becomes: maximize

$$H(f_1, \ldots, f_n) = -\sum_{i=1}^{n} f_i \log f_i \tag{5.2-3}$$

subject to two constraints: Eq. (5.2-1) and $\sum_{i=1}^{n} f_i = t$, where $t = \Delta \cdot g_T$ is a constant. Since Eq. (5.2-1) contains the noise term, a weighted sum of the

image entropy and the observation noise entropy is maximized in Frieden's approach.

The noise component may take either positive or negative values. Hence, the definition of noise entropy requires some care. The difficulty is overcome by applying additional *a priori* knowledge to the problem by assuming that a constant B is known such that

$$B = \max_j(-e_j). \tag{5.2-4}$$

In practice, B may be roughly estimated by setting it equal to 2σ, where σ is the standard deviation of the noise. According to Frieden, the quality of the restoration does not depend critically on B precisely satisfying Eq. (5.2-4); however, the results are best when Eq. (5.2-4) is indeed satisfied. We may now define a new nonnegative sequence

$$e_j' = e_j + B \geq 0 \tag{5.2-5}$$

and the noise entropy as

$$H_e = -\sum_{j=1}^{n} e_j' \log e_j'. \tag{5.2-6}$$

The restoration problem is solved by maximizing the weight sum

$$H(f_1, \ldots, f_n) + \rho H_e, \tag{5.2-7}$$

where the constant ρ is used to emphasize one of $H(f_1, \ldots, f_n)$ and H_ρ with respect to the other. Frieden recommends a value of $\rho = 20$ as about optimum for a wide range of object and noise situations.

Maximization of Eq. (5.2-7) is carried out subject to satisfying the following two equalities:

$$d_j = \sum_{i=1}^{n} A_{ji} f_i + e_j' - B, \tag{5.2-8}$$

$$\sum_{i=1}^{n} f_i = t. \tag{5.2-9}$$

The maximization can be carried out with Lagrange multipliers. We find the $m + n$ unknowns f_i $(i = 1, \ldots, n)$, e_j' $(j = 1, \ldots, m)$ that maximize the functional

$$K \triangleq H(f_1, \ldots, f_n) + \rho H_e + \sum_{j=1}^{m} \lambda_j \left(\sum_{i=1}^{n} A_{ji} f_i + e_j' - B - d_j \right) + \mu \left(\sum_{i=1}^{n} f_i - t \right), \tag{5.2-10}$$

where λ_j, $j = 1, \ldots, m$, and μ and $m + 1$ Lagrange multipliers.

Let $\hat{f}_i$ and $\hat{e}_j$ denote the optimum values of f_i and e'_j. Clearly, letting $\mathbf{f} \triangleq [f_1, \ldots, f_n]^T$, $\hat{\mathbf{f}} \triangleq [\hat{f}_1, \ldots, \hat{f}_n]^T$, $\mathbf{e} \triangleq [e_1, \ldots, e_m]^T$, and $\hat{\mathbf{e}} \triangleq [\hat{e}_1, \ldots, \hat{e}_m]^T$ we should have

$$\partial K/\partial f_i|_{f=\hat{f}} = 0, \tag{5.2-11}$$

$$\partial K/\partial e'_j|_{e'=\hat{e}} = 0. \tag{5.2-12}$$

Performing these differentiations, we obtain

$$\hat{f}_i = \exp\left(-1 + \mu + \sum_{j=1}^{m} \lambda_j A_{ji}\right) \tag{5.2-13}$$

and

$$\hat{e}_j = \exp(-1 + \lambda_j/\rho). \tag{5.2-14}$$

These solutions must satisfy the constraints given by Eqs. (5.2-8) and (5.2-9):

$$\sum_{i=1}^{n} A_{ji}\hat{f}_i + \hat{e}_j - B = d_j, \qquad j = 1, \ldots, m, \tag{5.2-15}$$

and

$$\sum_{i=1}^{n} \hat{f}_i = t. \tag{5.2-16}$$

The restored f_i is obtained by first substituting Eqs. (5.2-13) and (5.2-14) in Eqs. (5.2-15) and (5.2-16). The resulting $m + 1$ equations are solved for the $m + 1$ unknowns λ_j, $j = 1, \ldots, m$, and μ. These equations are highly nonlinear but, according to Frieden, are always solvable by an $(m + 1)$-dimensional Newton–Raphson method, provided B is large enough.

5.3 BURCH, GULL, AND SKILLING'S APPROACH [4]

Again let the required restored image have pixel values represented by nonnegative numbers $f_1, \ldots, f_n$ and the observed image data be given by

$$d_j = \sum_{i=1}^{n} A_{ji} f_i + e_j, \qquad j = 1, \ldots, m, \tag{5.3-1}$$

where the e'_js represent independent zero mean, σ_j^2 variance noise terms. Burch *et al.* attack the problem in a different way. They define

$$Q(f_1, \ldots, f_n) = \frac{1}{2}\sum_{j=1}^{m} \frac{1}{\sigma_j^2}\left(\sum_{i=1}^{n} A_{ji} f_i - d_j\right)^2. \tag{5.3-2}$$

Instead of the m constraint equations such as Eq. (5.3-1) Burch *et al.* use a single chi-squared, χ^2, statistic

$$Q(f_1, \ldots, f_n) = m/2. \tag{5.3-3}$$

The motivation for this constraint comes about from the central limit theorem [6], which states

$$\lim_{m\to 0} \frac{1}{m} \sum_{j=1}^{m} \frac{e_j^2}{\sigma_j^2} = 1. \tag{5.3-4}$$

Thus, provided that m is large, we would expect the true values of $f_1, \ldots, f_n$ to satisfy Eq. (5.3-3). This approach avoids a mathematically unwieldy proliferation of Lagrange multipliers and allows the development of an iterative technique applicable to large images. Instead of the functional K in Eq. (5.2-10), the following functional is maximized subject to $Q(f_1, \ldots, f_n) = m/2$ in Burch *et al.*'s approach:

$$J = -\sum_{i=1}^{n} f_i \log\left(\frac{f_i}{eA}\right) - \lambda Q(f_1, \ldots, f_n), \tag{5.3-5}$$

where A is a predetermined parameter and e the natural exponent. Expanding (5.3-5), we obtain

$$\begin{aligned} J &= -\sum_{i=1}^{n} f_i \log f_i - \lambda Q(f_1, \ldots, f_n) + (1 + \log A) \sum_{i=1}^{n} f_i \\ &= H(f_1, \ldots, f_n) - \lambda Q(f_1, \ldots, f_n) + (1 + \log A) \sum_{i=1}^{n} f_i \qquad (5.3\text{-}6) \\ &= H(f_1, \ldots, f_n) - \lambda Q(f_1, \ldots, f_n) + \mu \sum_{i=1}^{n} f_i, \qquad (5.3\text{-}7) \end{aligned}$$

where $\mu = (1 + \log A)$. If $f_1^*, \ldots, f_n^*$ maximize Eq. (5.3-7) subject to $Q(f_1, \ldots, f_n) = m/2$, then $f_1^*, \ldots, f_n^*$ would maximize $H(f_1, \ldots, f_n)$ subject to two constraints:

$$Q(f_1, \ldots, f_n) = m/2$$

and

$$\sum_{i=1}^{n} f_i = \sum_{i=1}^{n} f_i^*.$$

Noticing that

$$H(p_1, \ldots, p_n) = \frac{H(f_1, \ldots, f_n)}{\sum_{i=1}^{n} f_i} \log\left(\sum_{i=1}^{n} f_i\right)$$

we observe that the same $f_1^*, \ldots, f_n^*$ would maximize the entropy $H(p_1, \ldots, p_n)$ subject to the same two constraints. Here, $p_i = f_i / \sum_{i=1}^n f_i$ as before. The stationary point equation of Eq. (5.3-6) or Eq. (5.3-7) is

$$\nabla J = 0 \tag{5.3-8}$$

or

$$\log A - \log f_i - \lambda \frac{\partial}{\partial f_i} Q(f_1, \ldots, f_n) = 0 \tag{5.3-9}$$

or

$$(\mu - 1) - \log f_i - \lambda \frac{\partial}{\partial f_i} Q(f_1, \ldots, f_n) = 0. \tag{5.3-10}$$

Normally, we first attempt to solve an unconstrained maximization of J or its stationary point equation $\nabla J = 0$. The simplest such algorithm is steepest ascent, in which one performs a line search along the direction of ∇J. This is well known to be inefficient. The standard way to improve a steepest ascent algorithm is to use some variant of the conjugate gradient technique. Instead of using ∇J itself as the search direction, one uses a combination of this with previous gradient(s) chosen to give quick convergence if J is exactly quadratic in $f_1, \ldots, f_n$. Unfortunately, J in maximum entropy is highly nonquadratic, and conjugate gradients will also not be powerful.

Instead of searching along just one direction at a time, Burch *et al.* use a subspace of three directions, namely

$$(\mathbf{e}_1)_i \triangleq f_i \frac{\partial S}{\partial f_i}, \qquad \text{where for convenience let } S = -\sum_{i=1}^n f_i \log\left(\frac{f_i}{eA}\right), \tag{5.3-11}$$

$$(\mathbf{e}_2)_i \triangleq f_i \frac{\partial Q}{\partial f_i}, \tag{5.3-12}$$

$$(\mathbf{e}_3)_i \triangleq \sum_{j=1}^n f_i \frac{\partial^2 Q}{\partial f_i \, \partial f_j} f_j \frac{\partial J}{\partial f_j}, \tag{5.3-13}$$

where, according to the required stationary point equation $\nabla J = 0$ ($J = S - \lambda Q$), λ is necessarily given by

$$\lambda = \left(\frac{\sum_{i=1}^n f_i (\partial S / \partial f_i)^2}{\sum f_i (\partial Q / \partial f_i)^2} \right)^{1/2}. \tag{5.3-14}$$

Here the first direction $\mathbf{e}_1$ helps S to be maximized through $\partial S / \partial f_i$. The extra factor f_i has the operational characteristic of letting the algorithm

concentrate on intense areas of the image instead of areas already known to be faint and requiring little further attention. Likewise, the second direction $\mathbf{e}_2$ helps the desired value of Q to be reached, with a similar factor of f_i. These factors can be understood by using the entropy curvature $-\nabla\nabla S = -(\partial^2 S/\partial f_i\,\partial f_j) = \text{diag}[1/f_1, \ldots, 1/f_n]$ as the metric tensor defining lengths and angles in f space. The third direction $\mathbf{e}_3$ corresponds to the initial correction which a conjugate gradient maximization of J would make to the steepest ascent direction ∇J, provided $-\nabla\nabla S$ was being used as the metric.

Within this three-dimensional subspace, the iterative change to be made to f can be expressed as

$$\delta\mathbf{f} = x^1\mathbf{e}_1 + x^2\mathbf{e}_2 + x^3\mathbf{e}_3, \tag{5.3-15}$$

where suitable coefficients x^i $(i = 1, 2, 3)$ are to be determined. Burch *et al.* begin by constructing quadratic models for S and Q with respect to variables x^1, x^2, x^3 from the local gradients and curvatures, thus modeling

$$\begin{aligned}\tilde{S}(x) &= S + \nabla S\cdot\delta\mathbf{f} + \frac{1}{2}(\delta\mathbf{f})^T\nabla\nabla S(\delta\mathbf{f})\\ &= S + \sum_{i=1}^{3}(\nabla S, \mathbf{e}_i)x^i - \frac{1}{2}(\delta\mathbf{f})^T\,\text{diag}[1/f_1, \ldots, 1/f_n](\delta\mathbf{f})\\ &= S + \sum_{i=1}^{3}(\nabla S, \mathbf{e}_i)x^i - \frac{1}{2}\sum_{i,j=1}^{3}(\mathbf{e}_i^T\,\text{diag}[1/f_1, \ldots, 1/f_n]\mathbf{e}_j)x^ix^j,\end{aligned} \tag{5.3-16}$$

$$\begin{aligned}\tilde{Q}(x) &= Q + (\nabla Q, \delta f) + \frac{1}{2}(\delta\mathbf{f})^T\nabla\nabla Q(\partial\mathbf{f})\\ &= Q + \sum_{i=1}^{3}(\nabla Q, \mathbf{e}_i)x^i + \frac{1}{2}(\delta\mathbf{f})^TA'DA(\delta\mathbf{f})\\ &= Q + \sum_{i=1}^{3}(\nabla Q, \mathbf{e}_i)x^i + \frac{1}{2}\sum_{i,j=1}^{3}(\mathbf{e}_i^T\mathbf{A}^T\mathbf{D}\mathbf{A}\mathbf{e}_j)x^ix^j,\end{aligned} \tag{5.3-17}$$

where $\mathbf{A} = (A_{ji})_{m\times n}$, $\mathbf{D} = \text{diag}[d_1, \ldots, d_m]$.

In keeping with using $-\nabla\nabla S$ as the metric tensor in $\mathbf{f}$ space, Burch *et al.* define the length squared of the increment $\delta\mathbf{f}$ as

$$\begin{aligned}l^2 &= (\delta\mathbf{f})^T(-\nabla\nabla S)(\delta f)\\ &= \sum_{i,j=1}^{3}(\mathbf{e}_i^T\,\text{diag}[1/f_1, \ldots, 1/f_n]\mathbf{e}_j)x^ix^j.\end{aligned} \tag{5.3-18}$$

Starting with a flat iterate $f_j = A$, the control of the algorithm now passes into the subspace, where highly sophisticated processing can be performed

on the 26 defining scalars S, Q, $(\nabla S, \mathbf{e}_i)$, $(\mathbf{e}_i^T \operatorname{diag}[1/f_1, \ldots, 1/f_n]\mathbf{e}_j)$, $(\nabla Q, \mathbf{e}_i)$, $(\mathbf{e}_i^T \mathbf{A}^T \mathbf{D} \mathbf{A} \mathbf{e}_j)$, $i, j = 1, 2, 3$.

The first "control" step is to rotate the coordinate system within the subspace to diagonalize the symmetric matrix

$$(\mathbf{e}_i^T \operatorname{diag}[1/f_1, \ldots, 1/f_n]\mathbf{e}_j)_{3\times 3}.$$

This enables the algorithm to be protected against accidental linear dependence of the search directions by discarding eigenvectors corresponding to unusually small eigenvalues of $(\mathbf{e}_i^T \operatorname{diag}[1/f_1, \ldots, 1/f_n]\mathbf{e}_j)_{3\times 3}$.

Assume $\mathbf{R} = [\mathbf{r}_1, \mathbf{r}_2, \mathbf{r}_3]$ is a 3×3 rotational matrix, i.e., orthonormal with $\det(\mathbf{R}) = 1$ such that

$$\mathbf{R}^T(\mathbf{e}_i^T \operatorname{diag}[1/f_1, \ldots, 1/f_n]\mathbf{e}_j)_{3\times 3}\mathbf{R} = \operatorname{diag}[\lambda_1, \lambda_2, \lambda_3] \tag{5.3-19}$$

or after rearrangement

$$([\mathbf{e}_1, \mathbf{e}_2, \mathbf{e}_3]\mathbf{R})^T \operatorname{diag}[1/f_1, \ldots, 1/f_n]([\mathbf{e}_1, \mathbf{e}_2, \mathbf{e}_3]\mathbf{R})$$

$$= \operatorname{diag}[\lambda_1, \lambda_2, \lambda_3](\operatorname{diag}[1/\sqrt{f_1}, \ldots, 1/\sqrt{f_n}][\mathbf{e}_1, \mathbf{e}_2, \mathbf{e}_3]\mathbf{R})^T. \tag{5.3-20}$$

$$(\operatorname{diag}[1/\sqrt{f_1}, \ldots, 1/\sqrt{f_n}][\mathbf{e}_1, \mathbf{e}_2, \mathbf{e}_3]\mathbf{R}) = \operatorname{diag}[\lambda_1, \lambda_2, \lambda_3]. \tag{5.3-21}$$

It is clear that

$$\begin{aligned}
\lambda_1 &= \|\operatorname{diag}[1/\sqrt{f_1}, \ldots, 1/\sqrt{f_n}][\mathbf{e}_1, \mathbf{e}_2, \mathbf{e}_3]\mathbf{R}[1, 0, 0]^T\|^2 \geqslant 0, \\
\lambda_2 &= \|\operatorname{diag}[1/\sqrt{f_1}, \ldots, 1/\sqrt{f_n}][\mathbf{e}_1, \mathbf{e}_2, \mathbf{e}_3]\mathbf{R}[0, 1, 0]^T\|^2 \geqslant 0, \\
\lambda_3 &= \|\operatorname{diag}[1/\sqrt{f_1}, \ldots, 1/\sqrt{f_n}][\mathbf{e}_1, \mathbf{e}_2, \mathbf{e}_3]\mathbf{R}[0, 0, 1]^T\|^2 \geqslant 0.
\end{aligned} \tag{5.3-22}$$

Thus, from Eq. (5.3-22) it is clear that there is a zero eigenvalue $\lambda_i = 0$ if and only if

$$\operatorname{diag}[1/\sqrt{f_1}, \ldots, 1/\sqrt{f_n}][\mathbf{e}_1, \mathbf{e}_2, \mathbf{e}_3]\mathbf{r}_i = 0 \tag{5.3-23}$$

or

$$[\mathbf{e}_1, \mathbf{e}_2, \mathbf{e}_3]\mathbf{r}_i = 0 \tag{5.3-24}$$

or the search directions $\mathbf{e}_1$, $\mathbf{e}_2$, $\mathbf{e}_3$, are linearly dependent. Moreover, it is easy to verify that $\mathbf{r}_i$ is the eigenvector of

$$([\mathbf{e}_1, \mathbf{e}_2, \mathbf{e}_3]^T \operatorname{diag}[1/f_1, \ldots, 1/f_n][\mathbf{e}_1, \mathbf{e}_2, \mathbf{e}_3])_{3\times 3}$$

corresponding to zero eigenvalue $\lambda_i = 0$.

Let $\mathbf{y} = \mathbf{R}\mathbf{x}$. Then $\tilde{S}(\mathbf{x})$, $\tilde{Q}(\mathbf{x})$ becomes $\tilde{S}(\mathbf{y})$, $\tilde{Q}(\mathbf{y})$, respectively, where

$$\tilde{S}(\mathbf{y}) = S + [(\nabla S, \mathbf{e}_i)]_{3\times 1}^T \mathbf{R}^T \mathbf{y} - \tfrac{1}{2}\mathbf{y}^T \operatorname{diag}[\lambda_1, \lambda_2, \lambda_3]\mathbf{y}, \tag{5.3-25}$$

$$\tilde{Q}(\mathbf{y}) = Q + [(\nabla Q, \mathbf{e}_i)]_{3\times 1}^T \mathbf{R}^T \mathbf{y} + \tfrac{1}{2}\mathbf{y}^T \mathbf{R}^T (\mathbf{e}_i^T \mathbf{A}^T \mathbf{D} \mathbf{A} \mathbf{e}_j)_{3\times 3}\mathbf{R}\mathbf{y}. \tag{5.3-26}$$

If none of three eigenvalues λ_1, λ_2, λ_3 is small, letting $\mathbf{z} = \text{diag}[\sqrt{\lambda_1}, \sqrt{\lambda_2}, \sqrt{\lambda_3}]\mathbf{y}$, $\tilde{S}(\mathbf{u})$, $\tilde{Q}(\mathbf{y})$ becomes $\tilde{S}(\mathbf{z})$, $\tilde{Q}(\mathbf{z})$, respectively, where

$$\tilde{S}(\mathbf{z}) = S + [(\nabla S, \mathbf{e}_i)]_{3\times 1}^T \mathbf{R}^T \text{diag}[1/\sqrt{\lambda_1}, 1/\sqrt{\lambda_2}, 1/\sqrt{\lambda_3}]\mathbf{z} - \tfrac{1}{2}\mathbf{z}^T\mathbf{z}, \quad (5.3\text{-}27)$$

$$\begin{aligned}\tilde{Q}(\mathbf{z}) = Q &+ [(\nabla Q, \mathbf{e}_i)]_{3\times 1}^T \mathbf{R}^T \text{diag}[1/\sqrt{\lambda_1}, 1/\sqrt{\lambda_2}, 1/\sqrt{\lambda_3}]\mathbf{z} \\ &+ \tfrac{1}{2}\mathbf{z}^T \text{diag}[1/\sqrt{\lambda_1}, 1/\sqrt{\lambda_2}, 1/\sqrt{\lambda_3}]\mathbf{R}^T(\mathbf{e}_i^T\mathbf{A}^T\mathbf{D}\mathbf{A}\mathbf{e}_j)_{3\times 3}\mathbf{R} \\ &\cdot \text{diag}[1/\sqrt{\lambda_1}, 1/\sqrt{\lambda_2}, 1/\sqrt{\lambda_3}]\mathbf{z}. \quad (5.3\text{-}28)\end{aligned}$$

Introduce the second rotational matrix $\mathbf{V}$ such that

$$\begin{aligned}&\mathbf{V}^T \text{diag}[1/\sqrt{\lambda_1}, 1/\sqrt{\lambda_2}, 1/\sqrt{\lambda_3}]\mathbf{R}^T(\mathbf{e}_i^T\mathbf{A}^T\mathbf{D}\mathbf{A}\mathbf{e}_j)_{3\times 3}\mathbf{R} \\ &\quad \cdot \text{diag}[1/\sqrt{\lambda_1}, 1/\sqrt{\lambda_2}, 1/\sqrt{\lambda_3}]\mathbf{V} = \text{diag}[\mu_1, \mu_2, \mu_3]. \quad (5.3\text{-}29)\end{aligned}$$

Letting $\mathbf{u} = \mathbf{V}\mathbf{z}$, $\tilde{S}(\mathbf{z})$ and $\tilde{Q}(\mathbf{z})$ become $\tilde{S}(\mathbf{u})$ and $\tilde{Q}(\mathbf{u})$, respectively, where

$$\tilde{S}(\mathbf{u}) = S + [(\nabla S, \mathbf{e}_i)]_{3\times 1}^T \mathbf{R}^T \text{diag}[1/\sqrt{\lambda_1}, 1/\sqrt{\lambda_2}, 1/\sqrt{\lambda_3}]\mathbf{V}^T\mathbf{u} - \frac{1}{2}\mathbf{u}^T\mathbf{u}, \quad (5.3\text{-}30)$$

$$\tilde{Q}(\mathbf{u}) = Q + [(\nabla Q, \mathbf{e}_i)]_{3\times 1}^T \mathbf{R}^T \text{diag}[1/\sqrt{\lambda_1}, 1/\sqrt{\lambda_2}, 1/\sqrt{\lambda_3}]\mathbf{V}^T\mathbf{u} + \frac{1}{2}\sum_{i=1}^{3} \mu_i u_i^2. \quad (5.3\text{-}31)$$

If λ_3 is very small but λ_1, λ_2 are not so small, we let $y_3 = 0$ and

$$[z_1, z_2]^T = \text{diag}[\sqrt{\lambda_1}, \sqrt{\lambda_2}][y_1, y_2]^T;$$

then $\tilde{S}(y)$, $\tilde{Q}(y)$ become $\tilde{S}(z)$, $\tilde{Q}(z)$, where

$$\begin{aligned}\tilde{S}(\mathbf{z}) &= S + [(\nabla S, \mathbf{e}_i)]_{3\times 1}^T \mathbf{R}^T \begin{bmatrix} \text{diag}[1/\sqrt{\lambda_1}, 1/\sqrt{\lambda_2}][z_1, z_2]^T \\ 0 \end{bmatrix} - \frac{1}{2}\sum_{i=1}^{2} z_i^2 \\ &= S + \sum_{i=1}^{2} S_i z_i - \frac{1}{2}\sum_{i=1}^{2} z_i^2, \quad (5.3\text{-}32)\end{aligned}$$

$$\tilde{Q}(\mathbf{z}) = Q + \sum_{i=1}^{2} Q_i z_i + \frac{1}{2}\sum_{i,j=1}^{2} M_{ij} z_i z_j, \quad (5.3\text{-}33)$$

where S_i, Q_i, M_{ij} all could be explicitly determined.

Introduce the second rotational matrix $\mathbf{V}_{2\times 2}$ such that

$$V^T M V = \text{diag}[\mu_1, \mu_2]. \quad (5.3\text{-}34)$$

Letting $\mathbf{u} = V\mathbf{z}$, $\tilde{S}(\mathbf{z})$, $\tilde{Q}(\mathbf{z})$ become $\tilde{S}(\mathbf{u})$, $\tilde{Q}(\mathbf{u})$:

$$\tilde{S}(\mathbf{u}) = S + [S_1, S_2]^T \mathbf{V}^T \mathbf{u} - \tfrac{1}{2}\mathbf{u}^T\mathbf{u}, \tag{5.3-35}$$

$$\tilde{Q}(\mathbf{u}) = Q + [Q_1, Q_2]^T \mathbf{V}^T \mathbf{u} + \frac{1}{2}\sum_{i=1}^{2} \mu_i \mu_i^2. \tag{5.3-36}$$

In any other cases, the treatment is similar.

Now we attempt to maximize S subject to $Q = m/2$ within the $\mathbf{u}$-subspace. Here without loss of generality we could write

$$\tilde{S}(\mathbf{u}) = S + \sum S_i u_i - \frac{1}{2}\sum u_i^2, \tag{5.3-37}$$

$$\tilde{Q}(\mathbf{u}) = Q + \sum Q_i u_i + \frac{1}{2}\sum \mu_i u_i^2. \tag{5.3-38}$$

Since the symmetric matrix $(\mathbf{e}_i^T \mathbf{A}^T \mathbf{D}\mathbf{A}\mathbf{e}_j)_{3\times 3}$ is nonnegative, eigenvalues μ_i are nonnegative, too. Thus, most likely $\tilde{Q}(\mathbf{u})$ will have a minimum value $Q - \frac{1}{2}\sum Q_i^2 \mu_i$. If the minimum value exceeds the desired value $m/2$, it is impossible to satisfy the constraint $\tilde{Q} = m/2$. Accordingly, Burch *et al.* set the more modest constraint $\tilde{Q} = \tilde{Q}_0$,

$$\tilde{Q}_0 = \max\left(Q - \frac{1}{3}\sum Q_i^2/\mu_i, m/2\right) \tag{5.3-39}$$

which is always accessible within the $\mathbf{u}$ subspace.

Maximizing $\tilde{S}$ subject to $\tilde{Q} = \tilde{Q}_0$ is equivalent to maximizing $\tilde{S} - \tilde{\lambda}\tilde{Q}$ subject to $\tilde{Q} = \tilde{Q}_0$. It leads to

$$u_i = (S_i - \tilde{\lambda} Q_i)/(1 + \tilde{\lambda}\mu_i) \tag{5.3-40}$$

A binary search could be used to give the value of $\tilde{\lambda}$ which attains the aim of $\tilde{Q}(\mathbf{u}) = \tilde{Q}_0$.

However, the quadratic model for S will only be accurate locally, within some distance limit: $u^T u \leqslant l_0^2 \simeq 0.2\sum f_i$, the factor 0.2 being a dimensionless coefficient suggested by Burch *et al.* from their practical experience. As easily seen, the following holds.

$$\begin{aligned} l^2 &\triangleq \mathbf{x}^T (e_i^T \operatorname{diag}[1/f_1, \ldots, 1/f_n] e_j)_{3\times 3} \mathbf{x} \\ &= \mathbf{y}^T \operatorname{diag}[\lambda_1, \lambda_2, \lambda_3] \mathbf{y} \\ &= \mathbf{z}^T \mathbf{z} \\ &= \mathbf{u}^T \mathbf{u}. \end{aligned} \tag{5.3-41}$$

So $\tilde{S}$ must be maximized subject to $\tilde{Q} = \tilde{Q}_0$ and an overrriding constraint $l^2 \leqslant l_0^2$. To satisfy the distance constraint, the algorithm normally uses the

same values of $\tilde{\lambda}$ and $\mathbf{u}$ as before, but the binary search is redirected toward the current value Q [see Eq. (5.3-38)] whenever $\tilde{\lambda}$ gives an increment with l^2 too large. This gives extra safety without changing the model parameters S, S_i, Q, q_i, μ_i.

When there is no sufficiently close increment, the distance constraint must be introduced explicitly via a second multiplier P, giving

$$\tilde{W} = \tilde{S} - \tilde{\lambda}\tilde{Q} - \tilde{\lambda}Pl^2 \qquad (P \geq 0), \tag{5.3-42}$$

since otherwise the first constraint $\tilde{Q} = \tilde{Q}_0$ could be drastically overriden by the second constraint $l^2 \leq l_0^2$. $\tilde{W}$ is maximized at

$$u_i = \frac{S_i - \tilde{\lambda}Q_i}{1 + \tilde{\lambda}(\mu_i + P)}. \tag{5.3-43}$$

P can be interpreted as a modification of $\tilde{Q}$ which increases its curvature components from μ_i to $\mu_i + P$, giving a revised model

$$\tilde{Q}_P = \tilde{Q} + \frac{1}{2}P\sum u_i^2. \tag{5.3-44}$$

With P invoked, $\tilde{\lambda}$ is searched toward $\tilde{Q} = \tilde{Q}_0$, but is redirected toward $\tilde{Q}_P = Q$ whenever l^2 is too large. For sufficiently large P, Burch *et al.* claimed that the binary search could always reach a result obeying

$$\tilde{Q}_0 \leq \tilde{Q} < \tilde{Q}_P \leq Q \tag{5.3-45}$$

and the smallest such P is used to give the final result $\mathbf{x}$.

All that remains is to increment $\mathbf{f}$ by the multiples x_i of the search directions while protecting against the very occasional stray nonnegative value.

Burch *et al.* also claimed that, in any case, the results are not sensitive to the precise value of the parameter A.

5.4 A DIFFERENTIAL EQUATION APPROACH TO MAXIMUM ENTROPY IMAGE RESTORATION [5]

In this section we develop a new algorithm for solving the maximum entropy image restoration problem. The problem is reduced to solving a system of ordinary differential equations with appropriate initial conditions. The choice of initial conditions closely relates to the satisfaction of constraints, and we show how the initial conditions are determined. The algorithm does not involve any optimization method. Instead of searching in the $(n + 1)$-dimensional space as required for most ME algorithms, our

approach relies on solving a one-dimensional search along a self-defined and easily mastered path. Moreover, an efficient algorithm is developed to handle the search. The computer restoration verifies the theory.

In subsection A of this section, the basic concepts for the maximum entropy restoration technique are given. This part includes the derivation of a system of differential equations defining a branch of solutions over which the one-dimensional search is performed. The section concludes with an analysis of the existence interval for λ, the search parameter. Subsection B deals mainly with the problem of selecting initial conditions so that the constraints imposed on the original formulation of the problem can be satisfied. A more comprehensive analysis of this subject is carried out in subsection C. The algorithm for solving the system of differential equations for the maximum entropy reconstruction problem is outlined in subsection D. Subsection E deals with the problem of adjusting a parameter in order to satisfy the constraint on the total image intensity embedded in the original problem formulation. In subsection F experiments in image reconstruction using the algorithm outlined in subsection E are described and results are presented.

A. Maximum Entropy, Stationary Point Equations, and Cauchy Problem of Differential Equations

Let the required reconstructed image have pixel values represented by positive numbers $f_1, \ldots, f_n$ which are to be determined, and on which the entropy

$$H(p_1, \ldots, p_n) = \sum_{i=1}^{n} p_i \log p_i, \qquad p_i = \frac{f_i}{\sum_{i=1}^{n} f_i}, \qquad i = 1, \ldots, n, \quad (5.4\text{-}1)$$

is defined. The entropy depends only on the distribution of gray levels in the image and not on the total intensity $\sum_{i=1}^{n} f_i$.

Let the observed image data be given by

$$d_j = \sum_{i=1}^{n} A_{ji} f_i + e_j, \qquad j = 1, \ldots, m, \quad (5.4\text{-}2)$$

where the e_j's represent independent zero mean, σ_j^2 variance noise terms. We define

$$Q(f_1, \ldots, f_n) = \frac{1}{2} \sum_{j=1}^{m} \frac{1}{\sigma_j^2} \left(\sum_{i=1}^{n} A_{ji} f_i - d_j \right)^2$$

$$= \frac{1}{2} (\mathbf{Af} - \mathbf{d})^T \operatorname{diag}[1/\sigma_1^2, \ldots, 1/\sigma_m^2] (\mathbf{Af} - \mathbf{d}) \frac{1}{2} \|\mathbf{Af} - \mathbf{d}\|_{\mathbf{D}}^2, \quad (5.4\text{-}3)$$

where $\mathbf{A} \triangleq [A_{ji}]_{m\times n}$, $\mathbf{f} \triangleq [f_1, \ldots, f_n]^T$, $\mathbf{d} \triangleq [d_1, \ldots, d_m]^T$, and $\mathbf{D} \triangleq \operatorname{diag}[1/\sigma_1^2, \ldots, 1/\sigma_m^2]$. Typical least-squares approaches would try to determine those values $f_1, \ldots, f_n$ which minimize $Q(f_1, \ldots, f_n)$. Rather than do this, we seek those $f_1, \ldots, f_n$ which maximize the entropy subject to the constraint

$$Q(f_1, \ldots, f_n) = m/2. \tag{5.4-4}$$

The motivation for this constraint comes about from the central limit theorem [6], which states

$$\lim_{m\to\infty} \frac{1}{m} \sum_{j=1} \frac{e_j^2}{\sigma_j^2} = 1.$$

Thus, provided that m is large, we would expect the true value of $f_1, \ldots, f_n$ to satisfy Eq. (5.4-4). The condition $Q = m/2$ now determines the set of feasible images $\mathbf{f}$ which pass the given statistical test for consistency with the actual image data $\{d_1, \ldots, d_m\}$.

Although any of the feasible images is acceptable as a reconstruction, the maximum entropy criterion selects that particular $\mathbf{f}$ which has the least configurational information, i.e., the one where the pixel values are least separated. Hence it can be looked on as a smoothing criterion. Of all reconstructions which fit the actual data $\{d_1, \ldots, d_m\}$, the maximum entropy solution thus gives uniquely safe and unprejudicial results.

Formally we are to maximize the entropy $H(p_1, \ldots, p_n)$ given the constraints $Q(f_1, \ldots, f_n) = m/2$ and $\sum_{i=1}^n f_i = t$ $(t > 0)$. We introduce the second constraint for two reasons. One is that the total intensity has a status different from individual pixel values. It does not contribute to the shape of the gray tone intensity function of the image $\mathbf{f}$. For the second reason we must look to the equality

$$H(p_1, \ldots, p_n) = \frac{H(f_1, \ldots, f_n)}{\sum_{i=1}^n f_i} - \log \sum_{i=1}^n f_i,$$

where $H(f_1, \ldots, f_n) = -\sum_i f_i \log f_i$. Introducing the second constraint $\sum_i f_i = t$, we obtain a linear relation between $H(f_1, \ldots, f_n)$ and $H(p_1, \ldots, p_n)$ enabling us to treat $H(f_1, \ldots, f_n)$ instead of $H(p_1, \ldots, p_n)$, the first one being much more tractable. Anyway, this constraint is not very strict, and it may be varied to obtain any required total intensity.

From the relation between $H(p_1, \ldots, p_n)$ and $H(f_1, \ldots, f_n)$ it is easily seen that the following three problems are equivalent to each other:

Problem 1. $\max H(p_1, \ldots, p_n)$

subject to $\quad Q = m/2, \quad \sum_i f_i = t.$

Problem 2. $\max H(f_1, \ldots, f_n)$

subject to $\quad Q = m/2, \quad \sum_i f_i = t.$

Problem 3. $\max[H(f_1, \ldots, f_n) + \mu \sum_i f_i - \lambda Q(f_1, \ldots, f_n)]$

subject to $\quad Q = m/2, \quad \sum_i f_i = t.$

Instead of solving problem 3, we solve the following problem:

Problem 4. $\max H[(f_1, \ldots, f_n) + \mu \sum_i f_i - \lambda Q(f_1, \ldots, f_n)]$

subject to $\quad Q = m/2.$

In problem 4 the total intensity is treated like a "free boundary condition." No specific value is assigned to it in advance. In fact, problem 4 is a very reasonable formulation of the maximum entropy image reconstruction problem. If $f_1^*, \ldots, f_n^*$ is a solution of problem 4, then it is also a solution of problems 1, 2, 3, with $t = \sum_i f_i^*$. Usually we are satisfied with the solution of problem 4. If not, we could adjust the parameter μ so that the solution of problem 4 has the required total intensity (see subsection F).

To solve problem 4 we need to consider the related unconstrained maximization problem.

Problem 5. $\max[H(f_1, \ldots, f_n) + \mu \sum_i f_i - \lambda Q(f_1, \ldots, f_n)]. \qquad (5.4\text{-}5)$

Let

$$J(f_1, \ldots, f_n; \mu, \lambda) = H(f_1, \ldots, f_n) + \mu \sum_i f_i - \lambda Q(f_i, \ldots, f_n)$$

Then problem 5 is to find maximal points of $J(f_1, \ldots, f_n; \mu, \lambda)$. The function $J(f; \mu, \lambda)$ is defined and continuous in the closed domain $\bar{E}$, where $E \triangleq \{f_i | f_i > 0, i = 1, \ldots, n\}$. When $\lambda \geqslant 0$ the continuous function J has a unique maximal point, which is finite since J tends to minus infinity as $\|\mathbf{f}\| \to \infty$ and is strictly concave due to the negative definiteness of its Jacobian $\nabla^2 J$:

$$\nabla^2 J = -\text{diag}[1/f_1, \ldots, 1/f_n] - \lambda \mathbf{A}^T \mathbf{D} \mathbf{A} < 0. \qquad (5.4\text{-}6)$$

As known, if the maximal point $\mathbf{f}^0$ is an inner point, i.e., $\mathbf{f}^0 \in E$, then the following stationary point equations hold:

$$\nabla J = -[\log f_1^0, \ldots, \log f_n^0]^T + (\mu - 1)\mathbf{h} - \lambda \mathbf{a}^T \mathbf{D}(\mathbf{A}\mathbf{f}^0 - \mathbf{d}) = 0, \quad (5.4\text{-}7)$$

where for abbreviation $\mathbf{h} \triangleq [1, \ldots, 1]^T_{1 \times n}$.

Conversely, if ∇J equals zero at a point $\mathbf{f}^0 \in E$ as $\lambda \geqslant 0$, then $\mathbf{f}^0$ must be a maximal point, as easily seen from Eq. (5.4-6).

In the following we will prove that Eq. (5.4-7) is always solvable as $\lambda \geqslant 0$. Thus, problem 5 is actually equivalent to Eq. (5.4-7) as $\lambda \geqslant 0$. The solution of Eq. (5.4-7) gives that unique maximal point required by problem 5 as $\lambda \geqslant 0$.

To prove that Eq. (5.4-7) is always (uniquely) solvable as $\lambda \geq 0$, all we need is to find such a path $\mathbf{f}(\lambda; \mu)$ in E, defined for $0 \leq \lambda < \infty$, that the gradient ∇J is identically equal to zero along it:

$$\nabla J(\mathbf{f}(\lambda; \mu); \mu, \lambda) \equiv 0, \qquad 0 \leq \lambda < \infty. \tag{5.4-8}$$

It is clear that Eq. (5.4-8) is equivalent to the following Eqs. (5.4-9) and (5.4-10).

$$\frac{d}{d\lambda} \nabla J(f(\lambda; \mu); \mu, \lambda) \equiv 0, \qquad 0 \leq \lambda < \infty, \tag{5.4-9}$$

$$\nabla J(\mathbf{f}(0; \mu); \mu, 0) = 0. \tag{5.4-10}$$

It is also clear that Eq. (5.4-9) is equivalent to the following differential equations for $\mathbf{f}(\lambda; \mu)$ (by working out the derivative $d\nabla J/d\lambda$):

$$\nabla^2 J(\mathbf{f}; \mu, \lambda)\, d\mathbf{f}/d\lambda = \partial Q(\mathbf{f}), \qquad 0 \leq \lambda < \infty, \tag{5.4-11}$$

and Eq. (5.4-10) directly gives $\mathbf{f}(0; \mu)$ as

$$\mathbf{f}(0; \mu) = \exp(\mu - 1)\mathbf{h}, \tag{5.4-12}$$

where $\mathbf{h}$ equals $[1, \ldots, 1]^T_{1 \times n}$.

Thus, the stationary point equation is always (uniquely) solvable as $\lambda \geq 0$ if the following Cauchy problem of differential equations defines a solution curve in E for $0 \leq \lambda < \infty$:

$$\begin{aligned} \nabla^2 J\, d\mathbf{f}/d\lambda &= \nabla Q, \\ \mathbf{f}|_{\lambda = 0} &= \exp(\mu - 1)\mathbf{h}. \end{aligned} \tag{5.4-13}$$

This is proved in Theorem 1 of the Appendix. Having shown that the unconstrained maximization problem 5 has the form of Eq. (5.4-13), we are ready to consider the variety of computing schemes available to solve it.

To solve the maximum entropy image reconstruction problem, the only thing left is to select suitable initial conditions for the Cauchy problem, Eq. (5.4-13), in order for the constraint $Q = m/2$ to be reached by the solution curve. For this we need to know more about the solution curve of Eq. (5.4-13). We discuss this in the next section.

B. Properties of Eq. (5.4-13)

In this subsection we define the sets giving the μ's for which a maximum entropy solution satisfying the constraint $Q = m/2$ can be found. Naturally, we are interested in the behavior of $Q(\mathbf{f}(\lambda; \mu))$ along the solution curve.

It is easy to see that

$$dQ(\mathbf{f}(\lambda;\mu))/d\lambda = (\nabla Q)^T d\mathbf{f}/d\lambda$$
$$\equiv (\nabla Q)^T(\nabla^2 J)^{-1}(\nabla Q). \tag{5.4-14}$$

In the following we prove that $Q(\mathbf{f}(\lambda;\mu))$ decreases strictly monotonically as λ increases unless the solution curve $\mathbf{f}(\lambda;\mu)$ shrinks into a single point $\exp(\mu-1)\mathbf{h}$. As a matter of fact, along the solution curve there are only two possibilities: either

$$\mathbf{f}(\lambda;\mu) \equiv \exp(\mu-1)\mathbf{h} \quad \text{and} \quad \nabla Q(\exp(\mu-1)\mathbf{h}) = 0, \tag{5.4-15}$$

or

$$\nabla Q(\mathbf{f}(\lambda;\mu)) \neq 0, \qquad 0 \leqslant \lambda < \infty. \tag{5.4-16}$$

Thus, when $\mathbf{f}(\lambda;\mu)$ does not shrink into a single point, the derivative $dQ(\mathbf{f}(\lambda;\mu))/d\lambda$ will always be negative because of (5.4-14), (5.4-16), and $(\nabla^2 J)^{-1} < 0$. As for (5.4-15) and (5.4-16) we can proceed as follows.

Suppose there exists a point $\mathbf{f}^* = \mathbf{f}(\lambda^*;\mu)$ along the solution curve such that

$$\nabla Q(\mathbf{f}^*) = 0. \tag{5.4-17}$$

Then $\mathbf{f}(\lambda;\mu)$ will coincide with the solution curve defined by the following Cauchy problem due to the uniqueness of the solution to

$$\nabla^2 J\, d\mathbf{f}/d\lambda = \nabla Q,$$
$$\mathbf{f}|_{\lambda=\lambda^*} = \mathbf{f}^*. \tag{5.4-18}$$

However, the solution curve of Eq. (5.4-18) obviously is a single point $\mathbf{f}^*$ due to Eq. (5.4-17) and the initial condition in Eq. (5.4-18). thus it holds

$$\mathbf{f}(\lambda;\mu) \equiv \mathbf{f}^*, \qquad 0 \leqslant \lambda < \infty. \tag{5.4-19}$$

Now it is not hard to see that Eq. (5.4-15) is valid since $\mathbf{f}(0;\mu) = \exp(\mu-1)\mathbf{h}$. Thus, we have proved

Theorem 5.4-1. The derivative $dQ(\mathbf{f}(\lambda;\mu))/d\lambda$ is always negative unless $\nabla Q(\exp(\mu-1)\mathbf{h}) = 0$.

In order for the solution curve $\mathbf{f}(\lambda;\mu)$ to satisfy the constraint $Q = m/2$, only those μ's need be considered which satisfy either

$$Q(\exp((\mu-1)\mathbf{h}) = m/2 \tag{5.4-20}$$

or

$$Q(\exp(\mu-1)\mathbf{h}) > m/2 \quad \text{and} \quad \nabla Q(\exp(\mu-1)\mathbf{h}) \neq 0. \tag{5.4-21}$$

If Eq. (5.4-20) holds, then $\exp(\mu - 1)\mathbf{h}$ solves problem 4. Otherwise, we need to select suitable μ's by means of Eq. (5.4-21) and then compute $\mathbf{f}(\lambda; \mu)$ by means of Eq. (5.4-13).

Let the sets U, V, W be defined as follows:

$$U = \{\mu : Q(\exp(\mu - 1)\mathbf{h}) = m/2\}, \tag{5.4-22}$$

$$V = \{\mu : Q(\exp(\mu - 1)\mathbf{h}) > m/2\}, \tag{5.4-23}$$

$$W = \{\mu : \nabla Q(\exp(\mu - 1)\mathbf{h}) \neq 0\}. \tag{5.4-24}$$

From the previous discussion it is clear that only those μ's which belong to U or $V \cap W$ can produce meaningful results.

C. *Computing the Sets U, V, and W*

In this subsection, we will investigate further the sets U, V, and W in order to determine initial values for which a maximum entropy solution satisfying the constraint can be found.

For abbreviation we let

$$\alpha = \exp(\mu - 1), \tag{5.4-25}$$

$$\mathbf{r} = \left[\sum_{i=1}^{n} A_{1i}/\sigma_1, \ldots, \sum_{i=1}^{n} A_{mi}/\sigma_m\right]^T, \tag{5.4-26}$$

$$\mathbf{S} = [d_1/\sigma_1, \ldots, d_m/\sigma_m]^T. \tag{5.4-27}$$

Then a direct computation yields

$$Q(\alpha\mathbf{h}) = a\alpha^2 + b\alpha + c, \tag{5.4-28}$$

where three coefficients a, b, c are as follows:

$$a = \tfrac{1}{2}\|\mathbf{r}\|^2 \tag{5.4-29}$$

$$b = -(\mathbf{r}, \mathbf{s}), \tag{5.4-30}$$

$$c = \tfrac{1}{2}\|\mathbf{s}\|^2. \tag{5.4-31}$$

By using the Schwartz inequality it is easily verified that $b^2 \leq 4ac$. In the following we prove that the expectation $E\{c\} \geq m/2$ and $(1/m)(c - \frac{1}{2}\|g\|^2) \to \frac{1}{2}$ with probability one as $m \to \infty$, where $\mathbf{g} \triangleq [\sum_{i=1}^{n} A_{1i}f_i/\sigma_1, \ldots, \sum_{i=1}^{m} A_{mi}f_i/\sigma_m]^T$ and the appearing f_i's are true image intensity values.

Let

$$\mathbf{u} = [e_1/\sigma_1, \ldots, e_m/\sigma_m]^T, \tag{5.4-32}$$

where the e_j's represent independent zero mean, σ_j^2 variance noise terms, as known in subsection A. From Eq. (5.4-2) we have

$$\mathbf{s} = \mathbf{g} + \mathbf{u} \tag{5.4-33}$$

and hence

$$\begin{aligned} E\{c\} &= \tfrac{1}{2}E\{\|\mathbf{g} + \mathbf{u}\|^2\} \\ &= \tfrac{1}{2}\|\mathbf{g}\|^2 + (\mathbf{g}, E\{\mathbf{u}\}) + \tfrac{1}{2}E\{\|\mathbf{u}\|^2\} \\ &= \tfrac{1}{2}\|\mathbf{g}\|^2 + m/2 \geqslant m/2. \end{aligned} \tag{5.4-34}$$

From Eq. (5.4-34) it is clear that $E\{c\} = m/2$ if and only if $\mathbf{g} = 0$.

As proved in Theorem 2 in the Appendix, if $\|g\|/m \to 0$ and $m \to \infty$, then with probability one

$$(1/m)(g, u) \to 0 \qquad \text{as } m \to \infty \tag{5.4-35}$$

and

$$(1/m)(c - \tfrac{1}{2}\|g\|^2) \to 0 \qquad \text{as } m \to \infty. \tag{5.4-36}$$

On the basis of this fact, if m is large and $\|g\|/m$ is small, then c can be rather safely replaced by $m/2 + \|g|^2/2$, which is never less than $m/2$. Hence in computing the sets U, V, and W, we assume $c \geqslant m/2$. In particular, we are interested in determining a nonempty set u or in determining the set intersection $V \cap W$ should $U = \varnothing$.

1. Computing the Set U

According to Eqs. (5.4-22), (5.4-25), and (5.4-28) the set U is determined as

$$U = \{1 + \log \alpha : a\alpha^2 + b\alpha + (c - m/2) = 0 \text{ with } \alpha > 0\}. \tag{5.4-37}$$

Case 1. $a > 0$, $b^2 > 4a(c - m/2)$, $b < 0$:

$$U = \begin{cases} \{1 + \log[(-b \pm \sqrt{b^2 - 4a(c - m/2)})/(2a)\}, & c > m/2, \\ \{1 + \log(-b/a)\}, & c = m/2. \end{cases} \tag{5.4-38}$$

Case 2. $a = 0$ ($\Rightarrow b = 0$), $c = m/2$:

$$U = \{(\infty, -\infty)\}. \tag{5.4-39}$$

In all other cases $U = \varnothing$, an empty set. Here the second case occurs very rarely. Thus in general U is empty or has at most two elements. This corresponds to no equientropy solution or at most two equientropy solutions for problem 4, respectively.

2. Computing the Set V When U Is Empty

The set V is determined as

$$V = \{1 + \log \alpha : a\alpha^2 + b\alpha + (c - m/2) > 0 \text{ with } \alpha > 0\}. \quad (5.4\text{-}40)$$

Since the set U is empty, the following cases exhaust all possibilities:

Case 1. $a > 0, b^2 - 4a(c - m/2) < 0.$
Case 2. $a > 0, b^2 - 4a(c - m/2) \geqslant 0, b \geqslant 0.$
Case 3. $a = 0 (\Rightarrow b = 0), c > m/2.$

It is easy to see that all three cases lead to the same V:

$$V = \{(-\infty, \infty)\}. \quad (5.4\text{-}41)$$

3. Computing the Set W

The set W is determined as:

$$W = \{1 + \log \alpha : \alpha(\mathbf{A}^T\mathbf{DAh}) \neq \mathbf{A}^T\mathbf{Dd} \text{ with } \alpha > 0\}. \quad (5.4\text{-}42)$$

From Eq. (5.4-42) it is clear that W equals $\{(-\infty, \infty)\}$ unless the $(n \times 1)$-vector $\mathbf{A}^T\mathbf{Dd}$ has the same direction as the $(n \times 1)$-vector $\mathbf{A}^T\mathbf{DAh}$. The exceptional case occurs very rarely. Thus in general there holds

$$W = \{(-\infty, \infty)\}. \quad (5.4\text{-}43)$$

In summary, there are only two possibilities in general. Either U is not empty and thus problem 4 has at most two equientropy solutions. Or $V \cap W = \{(-\infty, \infty)\}$ and thus for any μ there hold

$$Q(\exp(\mu - 1)\mathbf{h} > m/2, \quad (5.4\text{-}44)$$

$$\Delta Q(\exp(\mu - 1)\mathbf{h}) \neq 0. \quad (5.4\text{-}45)$$

As known from Theorem 5.4-1, Eq. (5.4-45) assures

$$dQ(\mathbf{f}(\lambda; \mu))/d\lambda < 0 \qquad \text{as } \lambda \geqslant 0, \quad (5.4\text{-}46)$$

where $\mathbf{f}(\lambda; \mu)$ is the unique solution of the Cauchy problem, Eq. (5.4-13). Intuitively, from Eq. (5.4-44) we would like to choose such a μ that $Q(\exp(\mu - 1)\mathbf{h})$ is as close to $m/2$ as possible. When $-b/2a > 0$, we can simply choose that

$$\mu = 1 + \log(-b/2a), \quad (5.4\text{-}47)$$

because of $[dQ(\alpha\mathbf{h})/d\alpha]_{\alpha=-b/2a} = 0$.

From Eqs. (5.4-26), (5.4-27) and (5.4-29), (5.4-30) it is apparent that the condition, $-b/2a > 0$, is equivalent to $(r, s) > 0$. Notice that d_j and f_i are

related by

$$d_j = \sum_{i=1}^{n} A_{ji} f_i + e_j, \qquad j = 1, \ldots, m,$$

where all f_i are nonnegative, and the matrix $(A_{ji})_{n\times m}$ represents the blurring operation which occurred in the imaging process. The latter implies $A_{ji} \geq 0$ in most practical cases. Thus, $(\mathbf{r}, \mathbf{s}) > 0$ will hold whenever the noise is not too large.

D. Algorithm for Solving Differential Equations

In this subsection the algorithm for solving the system of differential equations (5.4-13) is presented. As mentioned in the introduction, we do a search along the solution curve by varying the parameter λ, starting with $\lambda_0 = 0$. A satisfactory solution is found when $Q(\mathbf{f}(\lambda; \mu))/(m/2)$ is sufficiently near 1. For each λ a large system of linear equations must be solved. This is done by making extensive use of the properties of the coefficient matrix and applying the Gauss-Seidel algorithm [7], which is an iterative technique providing fast convergence.

Suppose that the U is empty, i.e., problem 4 has no equientropy solution, and moreover an appropriate μ has been chosen from the intersection $V \cap W$. From differential equations (5.4-13) we have the following discretized iterative equations:

$$\begin{cases} \mathbf{f}^0 = \exp(\mu - 1)\cdot\mathbf{h}, \\ k \geq 0: \quad (\mathbf{F}^k + \lambda_k \mathbf{A}^T\mathbf{D}\mathbf{A})(\mathbf{f}^{k+1} - \mathbf{f}^k) = -(\lambda_{k+1} - \lambda_k)\mathbf{A}^T\mathbf{D}(\mathbf{A}\mathbf{f}^k - \mathbf{d}), \end{cases} \tag{5.4-48}$$

where $\mathbf{F}^k = \operatorname{diag}[1/f_1^k, \ldots, 1/f_n^k]$, $\lambda_0 = 0$, and $\lambda_{k+1} > \lambda_k$. When all $|\lambda_{k+1} - \lambda_k|$ are small enough, $\mathbf{f}^k$ will approximate $\mathbf{f}(\lambda_k; \mu)$ very well. Equation (5.4-48) can be written as follows:

$$\begin{cases} \mathbf{f}^0 = \exp(\mu - 1)\mathbf{h}, \\ k \geq 0: \quad (\mathbf{F}^k + \lambda_k \mathbf{A}^T\mathbf{D}\mathbf{A})\mathbf{f}^{k+1} = (2\lambda_k - \lambda_{k+1})\mathbf{A}^T\mathbf{D}\mathbf{A}\mathbf{f}^k \\ \qquad\qquad + \mathbf{h} + (\lambda_{k+1} - \lambda_k)\mathbf{A}^T\mathbf{D}\mathbf{d}. \end{cases} \tag{5.4-49}$$

This is a large linear system of equations. Fortunately, the coefficient matrix $(\mathbf{F}^k + \lambda_k \mathbf{A}^T\mathbf{D}\mathbf{A})$ is positive definite and symmetric. The Gauss-Seidel iterative scheme (see [7]) can then be used to solve Eq. (5.4-49) efficiently.

Let $\mathbf{P}$ represent the matrix $(\mathbf{F}^k + \lambda_k \mathbf{A}^T\mathbf{D}\mathbf{A})$. Let $\mathbf{b}$ represent the vector $(2\lambda_k - \lambda_{k+1})\mathbf{A}^T\mathbf{D}\mathbf{A}\mathbf{f}^k + \mathbf{h} + (\lambda_{k+1} - \lambda_k)\mathbf{A}^T\mathbf{D}\mathbf{d}$. Further let $\mathbf{x}$ be the $(k+1)$st estimate $\mathbf{f}^{k+1}$ of $\mathbf{f}(\lambda_{k+1}; \mu)$. For $m \geq 1$ we have the following Gauss-Seidel

iterative equations for solving $\mathbf{Px} = \mathbf{b}$:

$$\begin{cases} \mathbf{x}^{(0)} = \mathbf{f}^k, \\ x_i^{(m)} = \dfrac{1}{P_{ii}}\left[v_i - \sum_{j<i} P_{ij}x_j^{(m)} - \sum_{j>i} P_{ij}x_j^{(m-1)} \right], \qquad i = 1, \ldots, n. \end{cases} \tag{5.4-50}$$

It is proved (see [7]) that the convergence and the limit point are independent of the choice of $\mathbf{x}^{(0)}$. Thus $\lim \mathbf{x}^{(m)} = \mathbf{f}^{k+1}$. We choose $\mathbf{x}^{(0)} = \mathbf{f}^k$ since $\mathbf{f}^{k+1}$ should be near $\mathbf{f}^k$ when $|\lambda_{k+1} - \lambda_k|$ is small. This choice of $\mathbf{x}^{(0)}$ greatly speeds up the convergence of (5.4-50). Experiments indicate that in most cases only one iteration for each k is enough to obtain $\mathbf{f}^{k+1}$ from $\mathbf{f}^k$.

In the sequel we let

$$\begin{cases} \mathbf{L} = \mathbf{A}^T\mathbf{DA}, \\ \mathbf{p} = \mathbf{A}^T\mathbf{Dd}, \\ \mathbf{g}^k = \mathbf{Lf}^k, \qquad k = 0, 1, 2, \ldots. \end{cases} \tag{5.4-51}$$

Then from Eq. (5.4-49) it follows

$$k \geqslant 0: \qquad (\mathbf{F}^k + \lambda_k\mathbf{f}^{k+1} = (2\lambda_k - \lambda_{k+1})\mathbf{g}^k + \mathbf{h} + (\lambda_{k+1} - \lambda_k)\mathbf{p}, \tag{5.4-52}$$

$$k \geqslant 1: \qquad \mathbf{g}^{k+1} = \left(2 - \frac{\lambda_{k+1}}{\lambda_k}\right)\mathbf{g}^k + \frac{1}{\lambda_k}\left[\frac{f_1^k - f_1^{k+1}}{f_1^k}, \ldots, \frac{f_n^k - f_n^{k+1}}{f_n^k}\right]^T + \left(\frac{\lambda_{k+1}}{\lambda_k} - 1\right)\mathbf{p}. \tag{5.4-53}$$

The initial values $\mathbf{f}^0$, $\mathbf{g}^0$, $\mathbf{g}^1$ for Eqs. (5.4-52)–(5.4-53) are as follows:

$$\begin{aligned} \mathbf{f}^0 &= \exp(\nu - 1)\mathbf{h}, \\ \mathbf{g}^0 &= \mathbf{Lf}^0 = \exp(\mu - 1)\left[\sum_{i=1}^n L_{1i}, \ldots, \sum_{i=1}^n L_{ni}\right]^T, \\ \mathbf{g}^1 &= \mathbf{Lf}^1. \end{aligned} \tag{5.4-54}$$

Thus Eq. (5.4-54), which involves matrix calculations, is used to find $\mathbf{g}^0$, $\mathbf{g}^1$, and the recursive formula (5.4-53) involving only vector calculations is used for $\mathbf{g}^k$, $k \geqslant 2$.

Finally we summarize this subsection by giving the following easily implemented algorithm for solving the maximum entropy image reconstruction problem.

Step 1. If $U \neq \varnothing$ and $\mu \in U$, then there is an equientropy solution $\mathbf{f}^* = \exp(\mu - 1)\mathbf{h}$. Stop.

Step 2. Choose an appropriate $\mu \in V \cap W$ such that $Q(\exp(\mu - 1)\mathbf{h})$ is as small as possible.

Step 3. Set $k = 0$, $\lambda_k = 0$, $\mathbf{f}^k = \exp(\mu - 1)\mathbf{h}$, $\mathbf{g}^k = \mathbf{L}\mathbf{f}^k$, and $Q^k = Q(\mathbf{f}^k)$.
Step 4. If $|Q^k/(m/2) - 1| \leq \varepsilon$, then Stop. Here ε is a prescribed small positive number.
Step 5. Solve Eq. (5.4-49) for $\mathbf{f}^{k+1}$ by using Gauss-Seidel iterative scheme, Eq. (5.4-50).
Step 6. Compute $Q^{k+1} = Q(\mathbf{f}^{k+1})$.
Step 7. If k is large enough, Stop.
Step 8. If $|Q^{k+1}/(m/2) - 1| \leq \varepsilon$, then Stop.
Step 9. If $k \geq 1$, then compute $\mathbf{g}^{k+1}$ by Eq. (5.4-53), else $\mathbf{g}^{k+1} = \mathbf{L}\mathbf{f}^{k+1}$.
Step 10. If $Q^{k+1} > m/2$, then set $\delta\lambda > 0$, else set $\delta\lambda < 0$.
Step 11. Set $k = k + 1$, $\lambda_k = \lambda_{k-1} + \delta\lambda$.
Step 12. Goto Step 5.

In the experiments we consider only cases where the blurring given by the matrix **A** can be represented as a convolution between the undergraded image and a (regular) mask. By making full use of the fact that very few of the elements in the matrix **L** are nonzero for moderate mask sizes, it has been possible to construct a fast algorithm without resorting to Fourier transforms. If the blurring happens in the imaging processes, then the mask usually is small. For very large masks, however, the situation is different, and the possibility of saving time by use of Fourier transforms should be investigated. Equation (5.4-49), however, does not have a convolution form, so implementation of Fourier transforms is not straightforward.

E. Adjusting μ to Get the Required Total Intensity

Assume that the set U is empty and we have parameters μ_0 and λ_0 such that $\lambda_0 \geq 0$ and $|Q(\mathbf{f}(\lambda_0; \mu_0))/(m/2) - 1| \leq \varepsilon$. We are looking for a differentiable curve $\lambda = \lambda(u)$ passsing through (μ_0, λ_0), along which the Q values, $Q(\mathbf{f}(\lambda(\mu); \mu))$, are constant. In this case, adjusting the parameter μ will not affect the satisfaction of the constraint $|Q/(m/2) - 1| \leq \varepsilon$. Now along the required curve we should have two relations:

$$dQ(\mathbf{f}(\lambda(\mu); \mu))/d\mu = 0, \tag{5.4-55}$$

$$\nabla J(\mathbf{f}(\lambda(\mu); \mu); \mu, \lambda(\mu)) = 0, \tag{5.4-56}$$

the latter because $f(\lambda(\mu); \mu)$ is the stationary point of the function $J(\mathbf{f}; \mu, \lambda(\mu))$ as known before.

From (5.4-56) it is easy to derive that

$$\nabla^2 J(\mathbf{f}(\lambda(\mu); \mu); \mu, \lambda(\mu)) \frac{d\mathbf{f}(\lambda(\mu); \mu)}{d\mu} + h - \frac{d\lambda(\mu)}{d\mu} \nabla Q(\mathbf{f}(\lambda(\mu); \mu)) = 0$$

or

$$\frac{d\mathbf{f}(\lambda(\mu);\mu)}{d\mu} \equiv [\nabla^2 J(\mathbf{f}(\lambda(\mu);\mu))]^{-1}\left[\frac{d\lambda(\mu)}{d\mu}\nabla Q(\mathbf{f}(\lambda(\mu);\mu)) - h\right]. \tag{5.4-57}$$

Under the assumption $U = \varnothing$, we have that

$$V \cap W = \{(-\infty, \infty)\}, \tag{5.4-58}$$

which implies that

$$\nabla Q(\exp(\mu - 1))\mathbf{h} \neq 0. \tag{5.4-59}$$

As stated before [see Eqs. (5.4-15) and (5.4-16)], Eq. (5.4-56) implies that

$$\nabla Q(\mathbf{f}(\lambda(\mu);\mu)) \neq 0 \tag{5.4-60}$$

everywhere.

From (5.4-55) we have

$$[\nabla Q(\mathbf{f}(\lambda(\mu);\mu))]^T d\mathbf{f}(\lambda(\mu);\mu)/d\mu \equiv 0. \tag{5.4-61}$$

Combining (5.4-59), (5.4-60), and (5.4-61), we obtain

$$d\lambda(\mu)/d\mu \equiv [\nabla Q]^T[\nabla^2 J]^{-1}\mathbf{h}/[\nabla Q]^T[\nabla^2 J]^{-1}[\nabla Q], \tag{5.4-62}$$

where the differential curve passes through (μ_0, λ_0), i.e., $\lambda(\mu_0) = \lambda_0$.

Then, multiplying both sides of (5.4-57) by $\mathbf{h}^T$, it follows

$$\begin{aligned}\frac{d\sum_{i=1}^n f_i(\lambda(\mu);\mu)}{d\mu} &\equiv \mathbf{h}^T[\nabla^2 J]^{-1}\nabla Q \cdot \frac{d\lambda}{d\mu} - \mathbf{h}^T[\nabla^2 J]^{-1}\mathbf{h} \\ &\equiv \frac{([\nabla Q]^T[\nabla^2 J]^{-1}\mathbf{h})^2}{[\nabla Q]^T[\nabla^2 J]^{-1}[\nabla Q]} - \mathbf{h}^T[\nabla^2 J]^{-1}\mathbf{h}. \end{aligned} \tag{5.4-63}$$

Finally, we obtain the following Cauchy problem of $n + 2$ differential equations for adjusting μ to ge the required total intensity:

$$\begin{aligned}[\nabla^2 J]\frac{d\mathbf{f}(\lambda(\mu);\mu)}{d\mu} &= \frac{d\lambda(\mu)}{d\mu}[\nabla Q] - \mathbf{h}, \\ \frac{d\lambda(\mu)}{d\mu} &= \frac{[\nabla Q]^T[\nabla^2 J]^{-1}\mathbf{h}}{[\nabla Q]^T[\nabla^2 J]^{-1}[\nabla Q]}, \\ \frac{d\sum_{i=1}^n f_i(\lambda(\mu);\mu)}{d\mu} &= \frac{([\nabla Q]^T[\nabla^2 J]^{-1}\mathbf{h})^2}{[\nabla Q]^T[\nabla^2 J]^{-1}[\nabla Q]} - \mathbf{h}^T[\nabla^2 J]^{-1}\mathbf{h}, \\ \mathbf{f}|_{\mu=\mu_0} &= \mathbf{f}(\lambda_0, \mu_0), \\ \lambda|_{\mu=\mu_0} &= \lambda_0, \\ \sum_{i=1}^n f_i|_{\mu=\mu_0} &= \mathbf{h}^T\mathbf{f}(\lambda_0;\mu_0). \end{aligned} \tag{5.4-64}$$

The iterative scheme for solving (5.4-64) is as follows.

Given: μ_0, λ_0, $\mathbf{f}^0 = \mathbf{f}(\lambda_0; \mu_0)$, $t_0 = \mathbf{h}^T\mathbf{f}_0$, and $k \geq 0$:

$$\frac{\lambda_{k+1} - \lambda_k}{\mu_{k+1} - \mu_k} = \frac{[\nabla Q(\mathbf{f}^k)]^T[\nabla^2 J(\mathbf{f}^k; \mu_k, \lambda_k)]^{-1}\mathbf{h}}{[\nabla Q(\mathbf{f}^k)]^T[\nabla^2 J(\mathbf{f}^k; \mu_k, \lambda_k)]^{-1}[\nabla Q(\mathbf{f}^k)]},$$

$$[\nabla^2 J](\mathbf{f}^k; \mu_k, \lambda_k)](\mathbf{f}^{k+1} - \mathbf{f}^k) = (\lambda_{k+1} - \lambda_k)[\nabla Q(\mathbf{f}^k)] - (\mu_{k+1} - \mu_k)\mathbf{h},$$

$$\frac{t_{k+1} - t_k}{\mu_{k+1} - \mu_k} = \frac{([\nabla Q(\mathbf{f}^k)]^T[\nabla^2 J(\mathbf{f}^k; \mu_k, \lambda_k)]^{-1}\mathbf{h})^2}{[\nabla Q(\mathbf{f}^k)]^T[\nabla^2 J(\mathbf{f}^k; \mu_k, \lambda_k)]^{-1}[\nabla Q(\mathbf{f}^k)] - \mathbf{h}^T[\nabla^2 J(\mathbf{f}^k; \mu_k, \lambda_k)]^{-1}\mathbf{h}}. \quad (5.4\text{-}65)$$

F. Experiments

Three source images were used in the experiments. The first one (Fig. 5.4-1) is a picture of a girl. The image size is 128×128 pixels, and the

Fig. 5.4-1. The 128×128 source image of a girl's face.

resolution in gray level is 8 bits. Five different degraded images were produced from this image. These images, which are input images for the algorithm, will be referred to as image 1 through image 5. Image 1 and image 2 were created by first convolving the source image with a 5×5 box filter (all kernel elements equal to unit). Random noise with zero mean and standard deviations of 4 and 40, respectively, was added to the blurred

image. This corresponds to signal-to-noise ratio (S/N) of 1000 and 10, respectively, for the resulting images. To get a stronger blurring, this source image was convolved with a 7×7 mask with the center 5×5 elements all equal to zero and the 24 border elements equal to unity. Noise with zero mean and standard deviations of 4 and 40, respectively, was added to the blurred image to produce image 3 and image 4. To test the ability of the algorithm to reconstruct an image when we have incomplete measurements, image 5 was created. It is identical to image 1, but the gray level is known only for every tenth pixel. For convenience that is done in a regular manner, producing the line pattern which can be seen in Fig. 5.4-2, where the five input images are shown. Data for these images are listed in Table 5.4-1.

Fig. 5.4.-2. Five degraded images. Images 1 to 4 show the source image of Fig. 5.4-1; (1) blurred with a 5×5 box filter and having additive Gaussian noise of 4; (2) blurred with a 5×5 box filter and having additive Gaussian noise of 40; (3) blurred with a 7×7 box filter and having additive Gaussian noise of 4; (4) blurred with a 7×7 box filter and having additive Gaussian noise of 40. Image 5 is image 1 sampled every tenth pixel by row and every tenth pixel by column.

Table 5.4-1
Input Images Created from Girl Source Image

Image	Size of mask	Standard deviations of noise	(S/N)	Sampling interval
Image 1	5×5	4.0	1000	1
Image 2	5×5	40.0	10	1
Image 3	7×7	4.0	1000	1
Image 4	7×7	40.0	10	1
Image 5	5×5	4.0	1000	10

The second source image (Fig. 5.4-3a) contains text and has size 480 columns by 100 lines. It was blurred by a 7×7 Gaussian filter with standard deviation of 5. Noise with a standard deviation of 4 was added to produce the input image shown in Fig. 5.4-3b. The third source image (Fig. 5.4-4a) is a 128×128 checkerboard image. The corresponding input image was produced by the same degradation process as was applied to the text image.

As stated by Eq. (5.4-25), the initial value for the solution vector $\mathbf{f}$ is $\mathbf{f}^0 = \alpha\mathbf{h}$, where $\alpha = \exp(\mu - 1)$. For fastest possible convergence α is chosen so that $Q(\alpha\mathbf{h})$ is the smallest possible (provided $U = \varnothing$); that is, we choose $\alpha > 0$ so that $dQ(\alpha, \ldots, \alpha)/d\alpha = 0$ [see Eq. (5.4-20)].

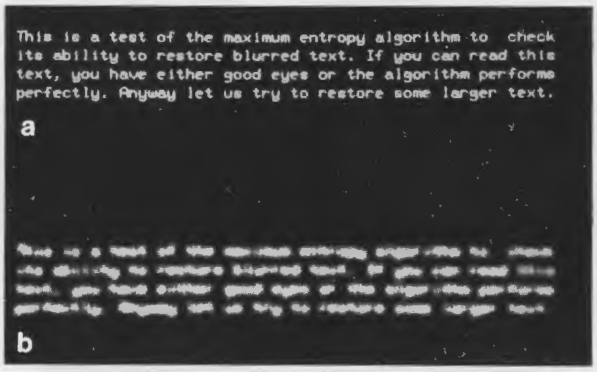

Fig. 5.4-3. (a) A 100×480 text source image. (b) The text source image blurred by a 7×7 Gaussian filter having a standard deviation of 5 and additive Gaussian noise with standard deviation 4.

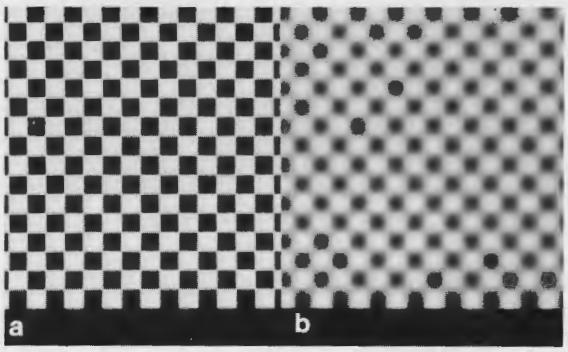

Fig. 5.4.-4. (a) A 128×128 checkerboard image. (b) The checkerboard image blurred by a 7×7 Gaussian filter having a standard deviation of 5 and additive Gaussian noise with standard deviation 4.

For each reconstruction the algorithm was run until the resulting Q was sufficiently near $Q = m/2$ (m is the number of data points, i.e., pixels). The number of iterations for each λ and step size in λ, $\delta\lambda = |\lambda_{k+1} - \lambda_k|$, were determined empirically, and the chosen values represent a reasonable, but in no way the best, choice. The optimal choice of $\delta\lambda$ also varies strongly with noise level. If the relative reduction in Q in one step is below a user-specified limit, the step size is doubled for the next step. This can save a great deal of time compared to keeping $\delta\lambda$ constant for a whole search. Indeed, in some cases it is quite necessary in order to be able to reach a solution in a reasonable time. One Gauss–Seidel iteration was enough to obtain f^{k+1} from f^k with satisfactory accuracy.

Table 5.4-2 gives an overview of some of the experiments run for the five input images generated from the Girl source image. K is the number of

Table 5.4-2
Data for Reconstruction of Girl Image

Image	K	$\delta\lambda_1$	$\delta\lambda_2$	λ-final	Q-init	Q-final	$m/2$	CPU
Image 1	1	0.2	0.2	0.2	769041	52588		1.36
Image 1	6	0.2	0.4	1.4	769041	10340		10.15
Image 1	12	0.2	0.4	3.8	769041	8381	8192	20.10
Image 2	1	4.0	4.0	4.0	15970	13539		1.36
Image 2	5	4.0	4.0	20.0	15970	8875		8.40
Image 2	9	4.0	4.0	36.0	15970	8379	8192	15.05
Image 3	1	0.2	0.3	0.2	643424	73208		2.50
Image 3	6	0.2	0.4	1.6	643424	11845		18.10
Image 3	10	0.25	0.5	4.0	643424	8423	8192	30.15
Image 4	1	4.0	4.0	4.0	14715	12814		2.50
Image 4	4	4.0	4.0	16.0	14715	9473		12.40
Image 4	8	4.0	4.0	32.0	14715	8412	8192	24.00
Image 5	1	0.5	0.5	0.5	77151	47400		1.45
Image 5	8	0.5	1.0	5.5	77151	3777		14.30
Image 5	15	0.5	1.0	12.5	77151	825	820	26.20

steps. $\delta\lambda_1$ is the initial step size in λ and $\delta\lambda_2$ is the final step size. Q-init is the initial Q value computed from the flat (constant) image which is the starting image. CPU is the VAX 11/780 CPU time in minutes and seconds. The corresponding images are shown in Figs. 5.4.5 to 5.4-9 for image 1 through image 5. The upper left image is the input image, upper right is the result after one step in λ, lower left is the intermediate result, and lower right is the final result.

Fig. 5.4-5. Restoration results for image 1. Image 1 is shown at the upper left. The restoration is shown after 1 step in λ at the upper right, after 6 steps in λ at the lower left, and after 12 steps in λ at the lower right.

Fig. 5.4-6. Restoration results for image 2. Image 2 is shown at the upper left. The restoration is shown after 1 step in λ at the upper right, after 6 steps in λ at the bottom left, and after 12 steps in λ at the lower right.

Fig. 5.4-7. Restoration results for image 3. Image 3 is shown at the upper left. The restoration is shown after 1 step in λ at the upper right, after 6 steps in λ at the lower left, and after 12 steps in λ at the lower right.

Fig. 5.4-8. Restoration results for image 4. Image 4 is shown at the upper left. The restoration is shown after 1 step in λ at the upper right, after 6 steps in λ at the lower left, and after 12 steps in λ at the lower right.

Fig. 5.4-9. Restoration results for image 5. Image 5 is shown at the upper left. The restoration is shown after 1 step in λ at the upper right, after 6 steps in λ at the lower left, and after 12 steps in λ at the lower right.

Table 5.4.-3 shows some of the experimental data for the text image and checkerboard image. The corresponding reconstructed images are shown in Figs. 5.4-10 and 5.4-11, respectively.

Table 5.4-3
Reconstruction Data for Text and Checkerboard Images

Image	K	$\delta\lambda_1$	$\delta\lambda_2$	λ-final	Q-init	Q-final	$m/2$	CPU
Text	22	0.50	256.0	768.5	827968	24574	24000	3.13.00
Check	6	0.25	0.5	2.0	1935043	50248		18.00
Check	25	0.25	32768.0	98308.0	1935043	9297	8192	1.15.00

The overall results indicate very good performance in reconstruction of blurred images even in cases where we have very few measurements. The performance in the reconstruction of extremely noisy images seems to be a little poorer. The experiments indicate that the algorithm runs better in deblurring than in noise removal. In fact, if no noise was present, it would be possible (in principle at least) to obtain a perfect reconstruction (which in this case is a pure deconvolution or deblurring). In practice, however,

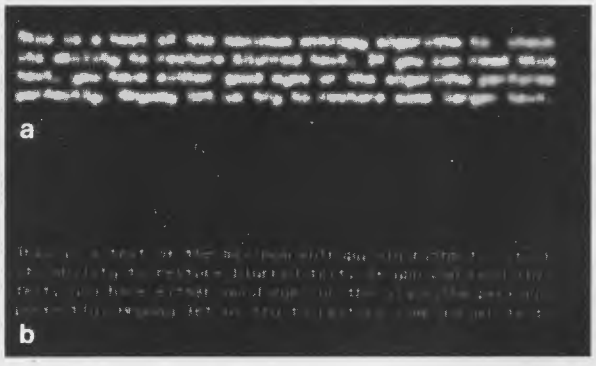

Fig. 5.4-10. Reconstruction of the text image. (a) Noisy blurred source image; (b) reconstructed image.

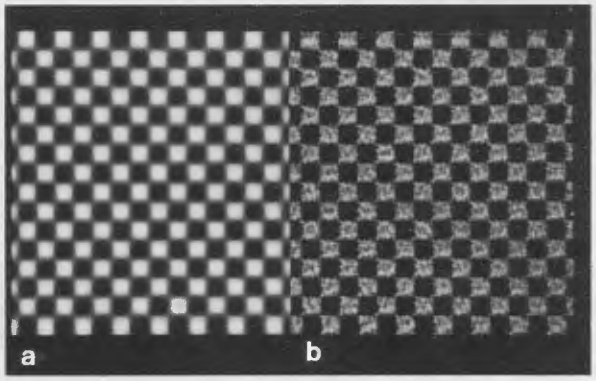

Fig. 5.4-11. Reconstruction of the degraded checkerboard image of Fig. 5.4-4. (a) Reconstruction after 6 steps in λ; (b) reconstruction after 25 steps in λ.

noise is always present, and even very small amounts of noise can cause the reconstructed data to fluctuate somewhat. The present algorithm, however, applies noise statistics [see Eq. (5.4-4)], which is the best way (statistically speaking) to deal with the noise.

Figures 5.4-5 to 5.4-9 indicate that in many cases it is not necessary to search all the way until Q reaches Q_0. The final results would not be very much different from the intermediate results obtained after 12 steps in λ as displayed in the figures. Thus, by accepting the intermediate results as the final reconstruction, a great deal of CPU time can be saved.

Table 5.4-3 reveals the importance of varying the step size $\delta\lambda$. The initial step size cannot be increased significantly from its present values, so a

constant step size would in many cases make practical applications impossible.

The checkerboard image was the only case where the result did not indisputably improve with the number of iterations. The average contrast between black and white squares did increase, but pixel values for the two regions overlap after 25 iterations (see Fig. 5.4-11), whereas this was not the case for just 6 iterations with a final λ of only 2.0 (shown in the same figure).

The experiments were run on a VAX-11/780 computer. Data for the experiments as well as CPU time consumed are listed in Tables 5.4-2 and 5.4-3. Though the general problem complexity is the square of the number of pixels, the computational complexity can in many cases (for instance, when the degradation matrix has a simple convolution form) be reduced to linear in the number of pixels. This is confirmed through experiments on a 256×256 image. For many applications CPU time is crucial. Taking into account the size of the problem, the CPU times listed in Tables 5.4-2 and 5.4-3 are very satisfactory. It is, however, evident that this time can be reduced even more if a better technique for finding an optimal or near-optimal $\delta\lambda$ for each step in the search along the path is developed.

5.5 CONCLUSION

We have briefly reviewed Frieden's approach and the Burch *et al.* approach to maximum entropy restoration. We have given a detailed description of a new differential equation approach to maximum entropy image restoration. We have performed and discussed an initial set of experiments with the differential equation approach.

The experimentation phase has not yet been completed. More combinations of the most essential parameters need to be investigated. To fully verify the potential of the algorithm, this more extensive experimentation should include:

(1) Testing more combinations of noise and blurring,
(2) Optimizing the search in λ,
(3) Possibly evaluating a better criterion for termination of the search process,
(4) Trying more source images, and
(5) Investigating possible time savings by use of Fourier transforms (for large masks).

A final assessment of the algorithm must wait for this work to be completed. However, the experiments run so far indicate that the algorithm

presented in this chapter is a very prospective tool in image reconstruction. In the most general case this reconstruction will require either an enormous storage capacity (the matrix $\mathbf{L} = \mathbf{A}^T\mathbf{D}\mathbf{A}$ has N^2 elements, where N is number of pixels in an image) or a substantial amount of CPU time (if all elements of $\mathbf{L}$ have to be computed every time they are used). However, in many practical applications simplifications are possible and the reconstruction can be done at a reasonable cost in CPU time without requiring excessive storage capacity.

APPENDIX

Theorem 1. A unique solution curve $\mathbf{f}(\lambda; \mu)$ is defined in E for $0 \leq \lambda < \infty$ by the following Cauchy problem of differential equations:

$$\begin{aligned} \nabla^2 J \, d\mathbf{f}/d\lambda &= \nabla Q, \\ \mathbf{f}|_{\lambda=0} &= \exp(\mu - 1)\mathbf{h}. \end{aligned} \tag{5.A-1}$$

Proof. Since the coefficient matrix $\nabla^2 J$ is negative definite and both $\nabla^2 J$ and ∇Q are analytic in E, Eq. (5.A-1) does define a unique solution curve $\mathbf{f}(\lambda; \mu)$ in E for $0 \leq \lambda < \alpha$ where α is some positive number or plus infinity. Thus all we need now is to prove that the solution curve could be extended whenever $\alpha < \infty$.

Suppose $\alpha < \infty$. We are to prove first that the solution curve $\mathbf{f}(\lambda; \mu)$ tends to a point $\mathbf{f}^* \in E$ as λ approaches α from below and the limit point $\mathbf{f}^*$ satisfies the stationary point equations, Eq. (5.4-7). Then the solution curve $\mathbf{f}(\lambda; \mu)$ is extended beyond α by the solution curve of the following Cauchy problem:

$$\begin{aligned} \nabla^2 J \, d\mathbf{f}/d\lambda &= \nabla Q, \\ \mathbf{f}|_{\lambda=\alpha} &= \mathbf{f}^*. \end{aligned} \tag{5.A-2}$$

Along the solution curve $\mathbf{f}(\lambda, \mu)$ we have

$$\nabla J(\mathbf{f}(\lambda; \mu); \mu, \lambda) \equiv 0, \qquad 0 \leq \lambda < \alpha. \tag{5.A-3}$$

Premultiplying Eq. (5.A-3) with $\mathbf{f}^T(\lambda; \mu)$ yields

$$\begin{aligned} \mathbf{f}^T \nabla J &\equiv -\sum_i f_i \log f_i + (\mu - 1)\sum_i f_i - \lambda \mathbf{f}^T(\mathbf{A}^T\mathbf{D}\mathbf{A})\mathbf{f} + \lambda \mathbf{f}^T\mathbf{A}^T\mathbf{D}\mathbf{d} \\ &\equiv 0, \qquad 0 \leq \lambda < \alpha, \end{aligned} \tag{5.A-4}$$

where for abbreviation the arguments in $\mathbf{f}(\lambda;\mu)$ are dropped. Equation (5.A-4) indicates that the norm $\|\mathbf{f}(\lambda;\mu)\|$ must be bounded as $\lambda \to \alpha - 0$. Otherwise $\mathbf{f}'(\lambda;\mu)\nabla J(\mathbf{f}(\lambda;\mu);\mu,\lambda)$ would go to $-\infty$ because of $\mathbf{f}^T(\lambda;\mu)(\mathbf{A}^T\mathbf{D}\mathbf{A})\mathbf{f}(\lambda;\mu) \geq 0$ and $-\sum f_i \log f_i + (\mu - 1)\sum f_i + \lambda \mathbf{f}^T\mathbf{A}^T\mathbf{D}\mathbf{A} \to -\infty$. The boundedness of $\|\mathbf{f}(\lambda;\mu)\|$ assures that each component $f_i(\lambda;\mu)$ has a positive lower bound as $\lambda \to \alpha - 0$. Otherwise the corresponding component of $\nabla J(\mathbf{f}(\lambda;\mu);\mu,\lambda)$ would go to ∞, as easily seen from Eq. (5.4-7). Therefore, not only the entire solution curve but also its limit point(s) as $\lambda \to \alpha - 0$ belong to E. Now it is clear that each limit point will satisfy Eq. (5.4-7) and hence coincide with that unique maximal point of J at α. If we denote the unique limit point by $\mathbf{f}^*$, then Eq. (5.A-2) does define a unique solution curve in E for some small interval $(\alpha - \delta, \alpha + \delta)$ with $\alpha - \delta \geq 0$ which coincides with the maximal point path of J as $\lambda \in (\alpha - \delta, \alpha + \delta)$. Hence the solution curve given by Eq. (5.A-2) coincides with $\mathbf{f}(\lambda;\mu)$ as $\lambda \in (\alpha - \delta, \alpha)$ and extends $\mathbf{f}(\lambda;\mu)$ beyond α.

Theorem 2. Assume that $\|\mathbf{g}\|/m \to 0$ as $m \to \infty$. Then with probability one,

$$\frac{1}{m}(\mathbf{g},\mathbf{u}) \to 0 \qquad \text{as } m \to \infty, \tag{5.A-5}$$

$$\frac{1}{m}\left(c - \frac{1}{2}\|\mathbf{g}\|^2\right) \to \frac{1}{2} \qquad \text{as } m \to \infty. \tag{5.A-6}$$

Proof. Let $x_m = (1/m)(\mathbf{g},\mathbf{u})$. It is easy to verify by means of $E\{u_i\} = 0$, $E\{u_i u_j\} = \delta_{ij}$, and the assumption $\|\mathbf{g}\|/m \to 0$ as $m \to \infty$ that

$$E\{x_m\} = 0, \tag{5.A-7}$$

$$\mathrm{Var}\{x_m\} = E\{x_m^2\} = \left(\frac{\|\mathbf{g}\|}{m}\right)^2 \to 0 \qquad \text{as } m \to \infty. \tag{5.A-8}$$

The latter will lead to $x_m \to 0$ as $m \to \infty$ with probability one by Chebychev's inequality (see [6], p. 151). This validates the first part of the theorem. To prove the second part we need to write $(1/m)(c - \frac{1}{2}\|\mathbf{g}\|^2)$ as

$$(1/m)(c - \tfrac{1}{2}\|\mathbf{g}\|^2) = x_m + (1/2m)\|\mathbf{u}\|^2. \tag{5.A-9}$$

The components u_j of $\mathbf{u}$ are independent, identically distributed random variables with zero mean and variance 1; thus $(1/m)\|\mathbf{u}\|^2 \to 1$ as $m \to \infty$ with probability one by the central limit theorem [6]. Combining this fact with $x_m \to 0$ as $m \to \infty$ with probability one, we obtain $(1/m)(c - \frac{1}{2}\|\mathbf{g}\|^2) \to \frac{1}{2}$ as $m \to \infty$ with probability one. This completes the second part of the theorem.

REFERENCES

1. E. T. Jaynes, Prior probabilities. *IEEE Trans. on Systems, Science and Cybernetics* **SSC-4**(3), 227–241 (1968).
2. E. T. Jaynes, The well-posed problem. *Foundation of Physics* **3**(4), 477–492 (1973).
3. B. R. Frieden, Restoring with maximum likelihood and maximum entropy. *J. Opt. Soc. Amer.* **G2**, 511–518 (1972).
4. S. F. Burch, S. F. Gull, and J. K. Skilling, Image restoration by a powerful maximum entropy method. *Computer Vision, Graphics, and Image Processing* **23**, 113–128 (1983).
5. X. Zhuang, E. Østevold, and R. M. Haralick, A differential equation approach to maximum entropy image reconstruction (to appear in *IEEE Trans. on Acoustics, Speech, and Signal Processing*).
6. W. Feller, "An Introduction to Probability Theory and Its Application, Vol. II," Second edition, John Wiley and Sons, Inc. 1971.
7. J. N. Franklin, "Matrix Theory," Prentice-Hall, Inc., 1968.